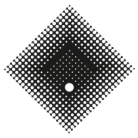
VICTORIA UNIVERSITY
MELBOURNE AUSTRALIA

Flexural performance of precast circular reinforced concrete members with intermediate connection filled with ultra-high-performance-concrete

This is the Published version of the following publication

Hamoda, Ahmed, Ahmed, Mizan, Ghalla, Mohamed, Liang, Qing and Abadel, Aref A (2023) Flexural performance of precast circular reinforced concrete members with intermediate connection filled with ultra-high-performance-concrete. Case Studies in Construction Materials, 19. ISSN 2214-5095 (In Press)

The publisher's official version can be found at https://www.sciencedirect.com/science/article/pii/S2214509523005661?via%3Dihub
Note that access to this version may require subscription.

Downloaded from VU Research Repository https://vuir.vu.edu.au/46990/

Case Studies in Construction Materials 19 (2023) e02386

Contents lists available at ScienceDirect

Case Studies in Construction Materials

journal homepage: www.elsevier.com/locate/cscm

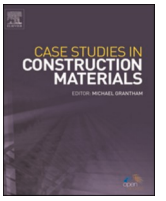

Flexural performance of precast circular reinforced concrete members with intermediate connection filled with ultra-high-performance-concrete

Ahmed Hamoda [a,*], Mizan Ahmed [b,*], Mohamed Ghalla [a], Qing Quan Liang [c], Aref A. Abadel [d]

[a] Civil Engineering Dept., Faculty of Engineering, Kafrelsheikh University, Kafrelsheikh, Egypt
[b] School of Civil and Mechanical Engineering, Curtin University, Kent Street, Bentley, WA 6102, Australia
[c] College of Sport, Health, and Engineering, Victoria University, PO Box 14428, Melbourne, VIC 8001, Australia
[d] Department of Civil Engineering, College of Engineering, King Saud University, Riyadh 11421, Saudi Arabia

ARTICLE INFO

Keywords:
Precast circular members
Flexural load
Ultra-high performance concrete
Finite element modeling, Nonlinear analysis

ABSTRACT

Precast Reinforced concrete (RC) columns with circular sections are increasingly being utilized in the construction of RC structures. This paper reports investigations into the flexural behavior of precast circular RC members with an intermediate connection filled with Ultra-High-Performance-Concrete (UHPC). Experimental program and results are described of twelve RC circular members tested under four-point loads up to collapse. Of the twelve columns, three of them are solid ones without intermediate connection, while nine of them are precast Normal Concrete (NC) panels connected with UHPC. The studied parameters are the existence of an intermediate connection (with and without connection), the ratio of longitudinal reinforcement (μ) ratio and the length of steel bars embedded in the UHPC connection (L_e). Three concrete types are used including Normal Concrete (NC), Strain Hardening Cementitious Composite (SHCC), and UHPC. Test results show that increasing the reinforcement ratio and the embedded length of the steel bars increases the strength and energy absorption of members. Finite element models (FEMs) developed using ABAQUS are presented for capturing the responses of RC columns incorporating different concrete types. The good agreement between computer simulation and experimental results suggests that the FEMs can be utilized to undertake further parametric studies with confidence.

1. Introduction

Reinforced Concrete (RC) columns are most commonly used in multistory buildings and car parks, and bridge piers as primary load-bearing members. However, in-situ RC columns often need significant formwork at the onsite and labor. On the contrary, precast concrete columns are cast in a controlled environment thus reducing onsite activities and offering economic benefits for a construction project [1]. Nonetheless, the delivery of the precast RC columns is limited to a certain length due to the limitation of the length of the transportation. Therefore, an intermediate connection is required for multiple precast columns in order to achieve the desired length.

* Corresponding authors.
E-mail addresses: ahmed_hamoda@eng.kfs.edu.eg (A. Hamoda), mizan.ahmed@curtin.edu.au (M. Ahmed).

https://doi.org/10.1016/j.cscm.2023.e02386
Received 19 June 2023; Received in revised form 4 August 2023; Accepted 9 August 2023
Available online 10 August 2023
2214-5095/© 2023 The Authors. Published by Elsevier Ltd. This is an open access article under the CC BY-NC-ND license (http://creativecommons.org/licenses/by-nc-nd/4.0/).

Besides, to speed up the construction of a large RC structure, it may be necessary to build from more than one side. Furthermore, due to the restricted lengths of deformed steel reinforcing bars beside the larger length of RC columns, the lap-spliced connections of steel reinforcing bars are often used in RC columns [2–4]. However, the stress transfer in the connecting zones is very critical and these zones may become potential weak spots [5]. Furthermore, the bonding between concrete and steel bars is one of the most governing parameters that control the structural behavior of precast RC members [6]. Considering wet joint provides better structural performance under different loading conditions than that modular connection [7], enhancing such joints may be achieved by using different types of High-Performance-Concrete (HPC) with superior performances in particular with tensile resistance.

Xu et al. [8] studied the seismic performance of precast bridge columns connected to footings using UHPC. The columns with UHPC exhibited ductile failure under cyclic loading. Graybeal [9] proposed UHPC connection between precast concrete bridge deck and tested their performance under large cyclic and static flexure and shear forces. No damage to the UHPC composite connection was observed during the test. Hussein et al. [10] proposed a novel shear key connection for precast prestressed box girder bridges made of UHPC. The proposed shear key connections subjected to direct shear, direct tension, and flexural tests were examined. Test results showed that the proposed shear key connections made of UHPC had higher load carrying capacity and improved strain distribution between the concrete components. Fang et al. [11] investigated the interfacial shear and flexural performance of innovative steel–precast UHPC composite beams. Test results showed that the composite beams with UHPC slabs exhibited significant improvements in the cracking load, ultimate load, horizontal interface slip capacity, and ductility compared with those with NC slabs.

The structural behavior of columns made of Ultra-High-Performance-Concrete (UHPC) strengthened with strips overlay was studied by Ganesh and Murthy [12]. It was reported that the application of UHPC increased the flexural capacity and fatigue life of the RC column; its performance was higher than that of the control column. The UHPC is characterized by high compressive strength, significant strain-hardening, good durability, and good toughness [13,14]. The flexural ductility of UHPC columns was studied by Tan et al. [15]. The UHPC enhanced the mechanical performance by about 180% and 450% for compressive and tensile strength, respectively. Tian et al. [16–19] examined the performance of concrete columns made of UHPC. It was found that columns made of UHPC exhibit higher load-carrying capacity and seismic performance than normal RC columns.

In recent decades, modified fiber-reinforced concrete materials have been developed, giving high strain-hardening performance under uniaxial tensile stresses [20]. One of these concrete materials is Strain-Hardening Cementitious Composite (SHCC). The good ductility of SHCC can be achieved by engineered micromechanical design [21]. The structural responses of RC columns that were strengthened by adding a near-surface SHCC layer were studied by Khan et al. [22]. The use of the SHCC as a strengthening technique enhanced the cracking load of the column by about 75% and its ultimate load by 120%. Cabboi et al. [23] presented test results on the delamination characteristics of hybrid SHCC concrete columns under dynamic loads. The natural frequency of the columns was found to decrease the progressive damage.

Based on the literature review it is evident that research on the flexural behavior of precast RC members with UHPC intermediate connection having different rebar ratios and connection lengths has not been undertaken yet. To overcome these limitations, this paper investigates the effects of different rebar ratios and connection lengths on the flexural behavior of RC members with UHPC intermediate connection. Therefore, this paper fills this research gap by experimentally and numerically investigating the structural performance of precast RC members with intermediate connection filled with UHPC subjected to flexural loading. This paper is organized as follows. A detailed description of the test program is given in Section 2. This is followed by the discussion of experimental results in Section 3. Section 4 presents the three-dimensional nonlinear FEMs developed using ABAQUS for the response simulation of the tested RC beams and experimental validation. Concluding remarks are given in Section 5.

2. Experimental program

The experimental investigation aimed to determine the structural responses of precast RC members with UHPC intermediate

Table 1
Details of tested specimens.

Group	Specimen`s ID	Concrete type	Construction joint length (mm)	L1 (mm)	Embedded Length (L_e)	Longitudinal Reinforcement (μ)
G1	C-NC	NC	————	————	————	6#10 mm (0.027)
	C-UHPC	UHPC	————	————	————	
	C-SHCC	SHCC	————	————	————	
G2	C-NC	NC	————	————	————	6#10 mm (0.027)
	U-0.027–15	UHPC	150	775	15D	
	U-0.027–22.5	UHPC	225	737.5	22.5D	
	U-0.027–30	UHPC	300	700	30D	
G3	C-NC	NC	————	————	————	6#10 mm (0.027)
	U-0.031–15	UHPC	150	775	15D	7#10 mm (0.031)
	U-0.031–22.5	UHPC	225	737.5	22.5D	
	U-0.031–30	UHPC	300	700	30D	
G4	C-NC	NC	————	————	————	6#10 mm (0.027)
	U-0.036–15	UHPC	150	775	15D	8#10 mm (0.036)
	U-0.036–22.5	UHPC	225	737.5	22.5D	
	U-0.036–30	UHPC	300	700	30D	

L_e = Embedded length; U = UHPC; D = Bar diameter; L1 = Outer length of the precast NC part

connection subjected to flexural loading using four-point loads. The four-point loads aimed to generate pure bending moment while neglecting shear forces at the intermediate connection. This loading type was selected to examine the connection zone under pure flexure with the absence of shear stresses. The influences of important parameters on the responses of RC beams with HPC were assessed, including the types of the filled concrete, steel reinforcing ratio, and embedded length (L_e). To evaluate and compare the effect of the variables, three RC solid member without intermediate connections were also prepared and tested.

2.1. Specimen details and test program

A total of twelve RC members, which were grouped into four groups, were constructed as summarized in Table 1 and tested in the structural lab of Kafrelsheikh University. All tested specimens had the same circular cross-section with a 150 mm diameter and an overall length of 1700 mm. The size and length of the tested specimens were designed based on the preliminary calculation of the capacity of the beam specimens in order to meet the capacity of the tested machine. The first Group was designed to ascertain the effects of concrete type on the behavior of RC members without intermediate connections as illustrated in Fig. 1(a). The specimens in Group 1 were labeled as C-NC, C-SHCC, and C-UHPC, which were made of NC, SHCC, and UHPC, respectively, as shown in Table 1. Specimen C-NC was added to all groups for comparison purposes. It should be noted that the main target of testing the column made of SHCC along with that made of UHPC was to understand the performance of different concrete types for construction joint.

The specimens in G2, G3, and G4 with intermediate connections are shown in Fig. 1(b) and Table 1. As given in Table 1, the reinforcement ratio; μ of the tested specimens in G2, G3, and G4 was 0.027, 0.031, and 0.036, respectively. Each group consisted of one NC slender specimen without an intermediate connection and three precast NC specimens with a UHPC intermediate joint. As illustrated in Fig. 1(b), the connection length varied as $L_e = 15D$, $22.5D$, and $30D$, where the D is referred to as the bar diameter. For example, the specimen U-0.027–15 refers to the specimen with a connection in G2 with a reinforcement ratio of 0.027 and its connection was filled with UHPC with L_e= 150 mm equal to $15D$.

2.2. Material properties and mix proportion

In order to study and enhance the mechanical performance of concrete, two types of high-performance fiber reinforced concrete were used to construct RC members, namely Strain Hardening Cementitious Composite (SHCC) and Ultra-High-Performance-Concrete (UHPC). The first one was UHPC characterized by superior compressive and tensile strength and the second one was SHCC which exhibited high strain hardening and excellent ductility. The NC mix was employed to be the master one. The mix proportions for each type are given in Table 2. The mixed design of SHCC was identical to the one reported by Hassan et al. [24].

The average compressive strengths obtained by testing 150 mm × 300 mm concrete cylinders were 30, 128, and 65 MPa for NC,

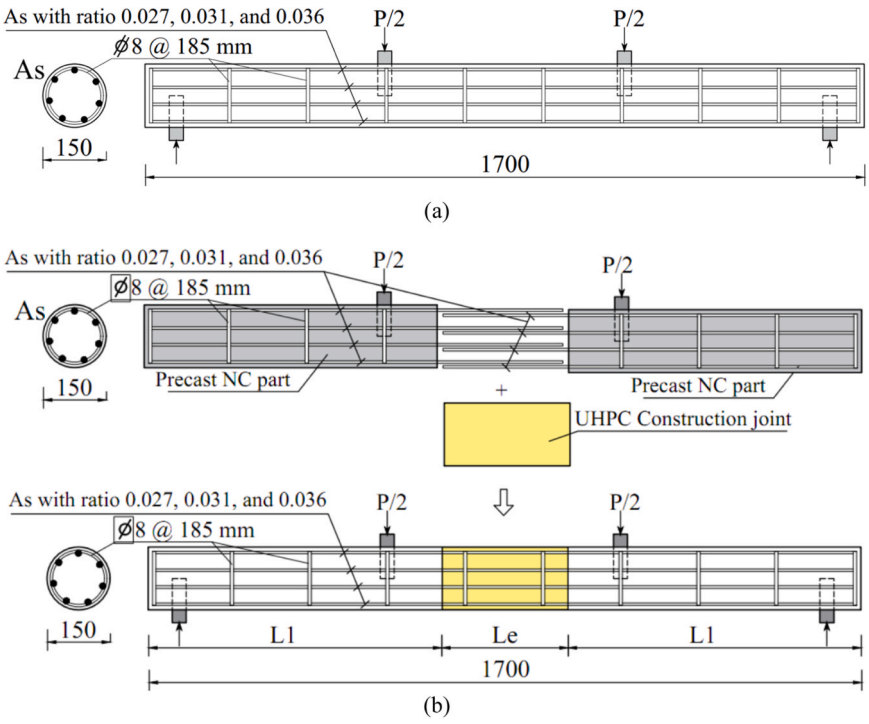

Fig. 1. Geometric and reinforcement details of the specimens: (a) Solid column without connection and (b) precast NC column with UHPC intermediate joint. (Units: mm).

UHPC, and SHCC, respectively, as provided in Table 2. Uniaxial axial tensile tests were performed on dog-bone specimens for NC and UHPC as shown in Fig. 2, to capture the tensile strengths. The uniaxial stress-strain curve for both NC and UHPC can be depicted in Fig. 2. The tensile strength of NC, UHPC, and SHCC was measured as 3.32, 7.01 and 7.14, respectively.

Two steel elements were used in this investigation, which were 8-mm diameter steel bars as ring stirrups with average grade 250/410 (Normal Milled Steel) and 10-mm diameter bars as longitudinal reinforcement with average grade 390/650 (High Tensile Strength). For each steel element, experimental tensile tests were carried out on three specimens. Fig. 3(a) shows the tensile coupon testing of a typical sample and Fig. 3(b) presents the average stress-strain relationships of the tested bars. The idealized stress-strain law was provided in order to be used in the FE simulation as shown in Fig. 3(b). The average values of modulus of elasticity were 196 and 210 GPa for 8-mm and 10-mm bars, respectively.

2.3. Casting and connecting preparation

Plastic longitudinal cylindrical formworks were prepared and used for casting the specimens as shown in Fig. 4(a). The casting of specimens with intermediate connections was conducted through two stages. In the first stage, NC was used for casting the two outer solid parts of the specimens as shown in Fig. 4(b). During the casting, some precast panels showed honeycomb due to the presence of the air bubble, which was then again patched with concrete manually, as can be seen in Fig. 4. However, this would not affect the mechanical performance of the members. After 24 h, the casted NC parts were de-molded and cured in a wet environment for 14 days. After that, they were allowed air drying. It can be seen from Fig. 4(c) that each pair of casted parts with equal length was oppositely positioned together to form the full specimens' length (1700 mm) incorporating the designed connection length (L_e). Parts of the connection were wrapped with an opening to enable casting UHPC in the horizontal position as demonstrated in Fig. 4(c).

2.4. Test setup and instrumentation

Fig. 5 shows the test set-up for the four-point load test of RC specimens. Four arched thick steel plates were used to enclose the specimens's circular geometry. Two of these plates were used as loading plates while the others were used as two hinged supports at the ends of the specimens. The full specimen's length was 1700 mm, including an overhanging length of 50 mm at each end as shown in Fig. 5(a,b). One Linear Variable Displacement Transducer (LVDT) was attached to the bottom of the specimens at the mid-span to record the vertical deflection during the loading process as shown in Fig. 5. Two electrical pi-gauges having a 50-mm gauge length were positioned at the connecting line between connection and specimens body to evaluate the expected vertical cracks as shown in Fig. 5(a). A load cell of 500 kN capacity was instrumented to measure the total load applied to the tested specimens. A digital data logger unit connected with its software was employed to record output data during the test for the load cell, LVDT, and measuring pi-gauges. The load on each specimen was applied incrementally. The development and propagation of cracks were marked up to the collapse of the tested specimens.

3. Test results and discussions

In this section, discussions are given on crack patterns, failure modes, load-deflection performance, elastic index, and absorbed energy. The experimental results of all specimens are given in Table 3, including the cracking load, its corresponding deflection, ultimate capacity, and maximum deflection at mid-span.

3.1. Crack pattern and failure modes

All specimens were tested under flexural moment from initial loading up to complete failure. The cracking patterns and collapse modes of all tested specimens can be seen in Figs. 6 to 9. Specimens in G1 were tested to failure and their results were used for comparison purposes. The main flexural behavior of such specimens can be seen in Fig. 6 in which the collapses of the specimens are shown.

For C-NC, the first visible hair flexural crack appeared at the bottom tension zone at a load value about of 24.1 kN (about 61.4% of P_u) as illustrated in Fig. 6(a). Then, cracks located at the bottom zone developed upward towards the upper compression side. When the loading was increased further, the crack width increased. When the major flexural crack width exceeded 1.5 mm, the specimens no longer sustained any more load so it failed. At failure, a sudden crushing of concrete between the two loading plates occurred as shown in Fig. 6(a). The ultimate load value was recorded as 39.2 kN. The final failure was flexural failure associated with concrete crushing.

Table 2
Mix proportions and properties of concrete.

Concrete	Cement (kg/m^3)	Fine aggregate (kg/m^3)	Coarse aggregate (kg/m^3)	Fly ash (kg/m^3)	Silica fume	Water/binder	Polypropylene (PP)/steel Fiber (%) in volume	HRWR (kg/m^3)	f_c` (MPa)
NC	350	700	1150	—	—	0.43	—	—	30
UHPC	900	1005	—	—	220	0.165	2.00	40.3	128
SHCC	1342	157.9	—	—	237	0.20	2.00	31.6	65

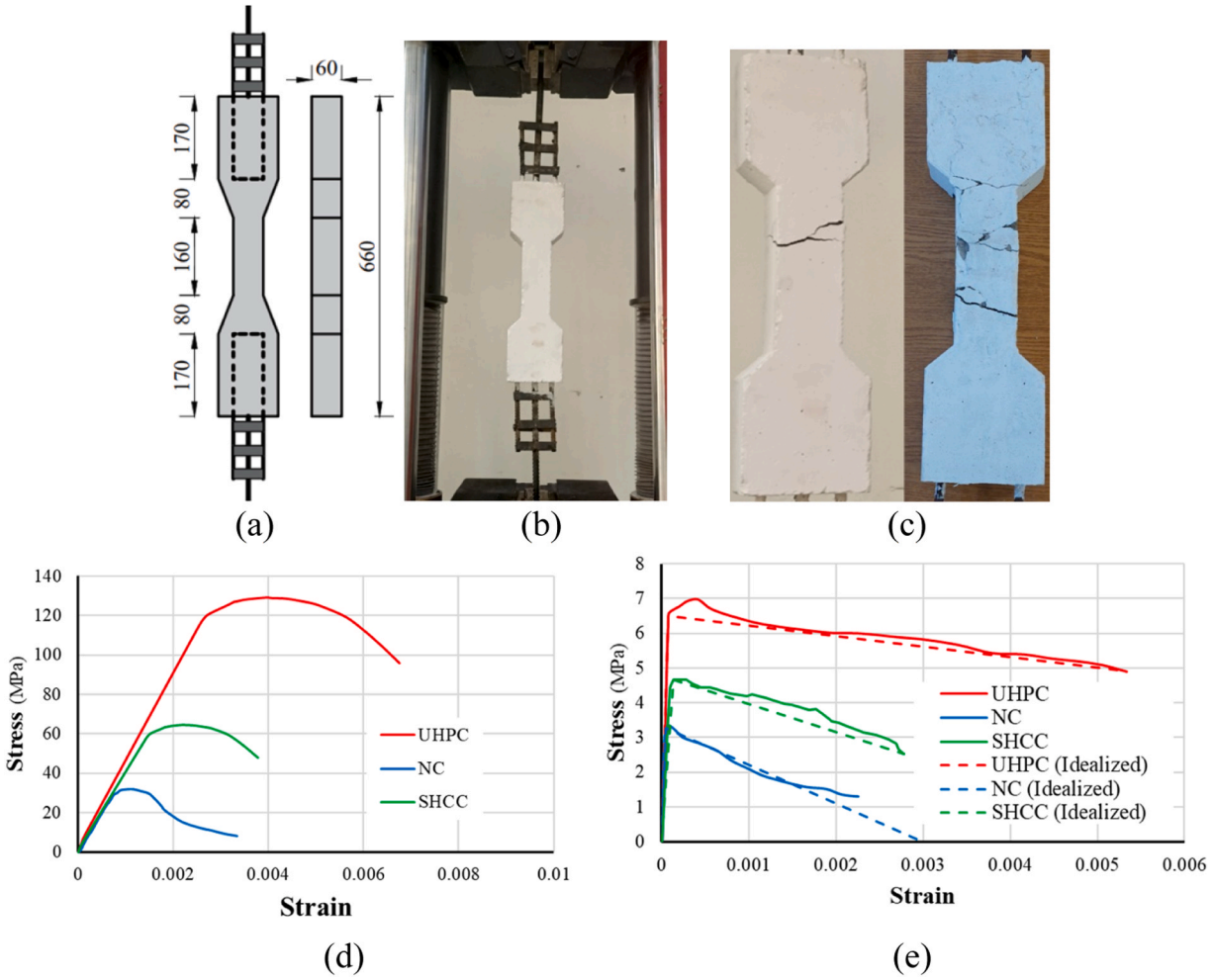

Fig. 2. Tension and compression behavior of NC and UHPC: (a) Concrete specimen dimensions, (b) Uniaxial tensile test, (c) failure tensile cracks (d) Compression stress-strain relationship (d) tension stress-strain relationship.

In order to assess the impact of HPC on such specimens, C-SHCC, and C-UHPC were constructed and tested. The cracking pattern of these specimens can be seen in Fig. 6(b) and (c), respectively. The first hair crack was recorded at the mid-span of the columns C-SHCC and C-UHPC at a cracking load of 30.05 kN and 32.6 kN, respectively as summarized in Table 3. The application of HPC enhanced the cracking load by about 25–35% compared to the NC counterpart. The increase in the first cracking load was due to the higher tensile performance of such specimens resulting from the bridge action of fibers. Same as the control specimen, the two specimens presented an ideal flexural performance. The width of the vertical flexural cracks increased and enlarged upward towards the upper zone as shown in Fig. 6. With the increase in the loading, more flexural cracks were seen at the bottom side, developed upward towards the region in compression. Finally, the tested specimens could not withstand any more load due to concrete crushing as shown in Fig. 6(b) and (c). The achieved ultimate capacities were 51.51 kN and 57.8 kN for specimens C-SHCC and C-UHPC, respectively, as tabulated in Table 3.

The specimens in G2 were designed to investigate the effects of the different embedded lengths on the performance of the specimens that had a reinforcement ratio of 0.027. The cracking pattern of the specimens in this group can be seen in Fig. 7. The flexural crack initialized at the interface surface between the NC specimens' body and UHPC connection part at loads leveled at 22.3 kN, 23.8 kN, and 28.5 kN for specimens with 15*D*, 22.5*D*, and 30*D* embedded length, respectively, as presented in Table 3. A few parallel vertical flexural cracks then developed in the NC part with no detection at the UHPC connection zone at the early loading stage as depicted in Fig. 7. The appearance of flexural-shear cracks was highlighted in the crack pattern of specimen U-0.027–30 as shown in Fig. 7(c). Both flexural and flexural-shear cracks extended upwards towards the loading plates and the cracks became wider as the applied load increased. Finally, the initial crack formed at the interface surface and widened up to the upper zone of the UHPC intermediate connection. For specimens U-0.027–15 and U-0.027–22.5, the sudden crushing of concrete was observed at the upper zone of the interface surface as shown in Fig. 7(a) and (b). These two specimens had ultimate loads of about 32.05 kN and 34.81 kN, respectively. On the other hand, the flexural-shear failure mode was presented for the 30D specimen as shown in Fig. 7(c). That may be

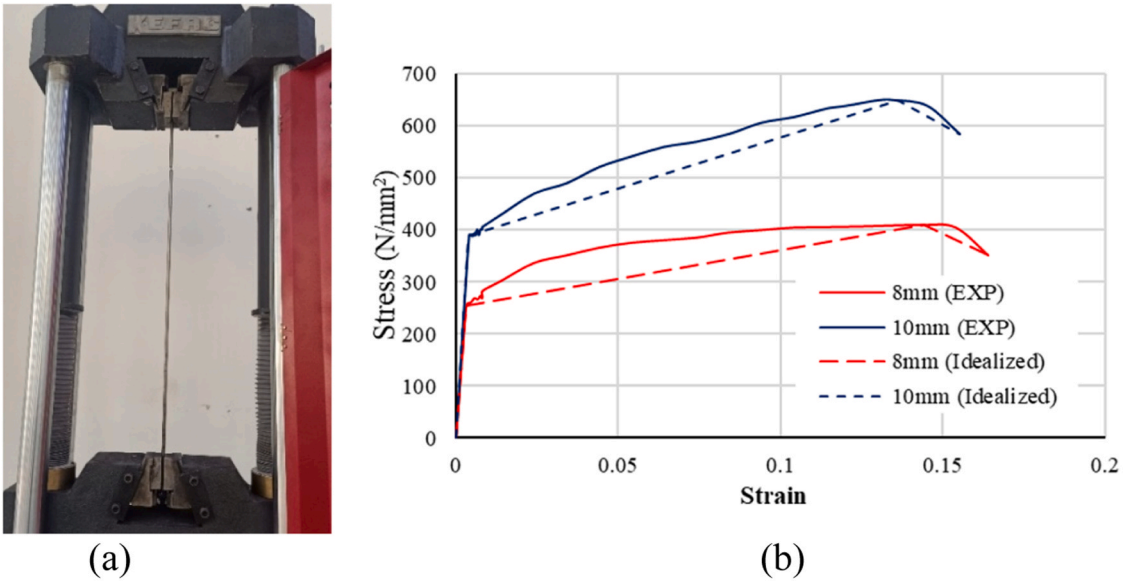

Fig. 3. Tensile test of steel bars: (a) tensile coupon test; (b) actual and idealized uniaxial stress-strain relationships.

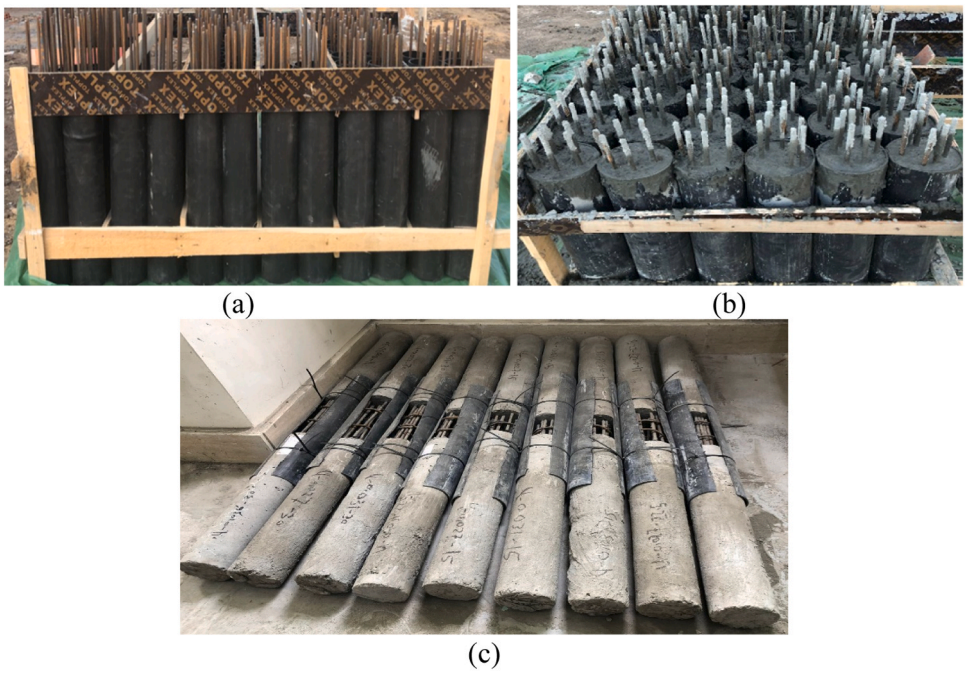

Fig. 4. Casting of specimens and preparation: (a) the formwork; (b) after casting; and (c) connecting the specimens.

due to the increase in the embedded length that shifted the cracks toward the supports. The final resistance of this specimen was recorded as about 36.22 kN, closer to the ultimate resistance of the master specimen.

Fig. 8 presents the cracking pattern of the specimens in the third group which was identical to the last group except a reinforcement ratio of 0.031 was used. Three UHPC connections with different embedded lengths were studied through specimens: U-0.031–15, U-0.031–22.5, and U-0.031–30. The first flexural vertical crack developed at the interface surface between the NC specimen panel and UHPC connection part at load of about 25.42, 29.6 and 32.94 kN, respectively, which was higher than that of the control NC specimen by about 5%, 11% and 14%, respectively as demonstrated in Fig. 8. Some shear-flexural cracks were seen to be initiated in NC panel and the number of cracks was higher than their counterparts tested in the previous group. With higher load values, one of the shear-flexural cracks developed with a wider appearance upward toward the loading plates. The failure occurred in the NC panel at the zone

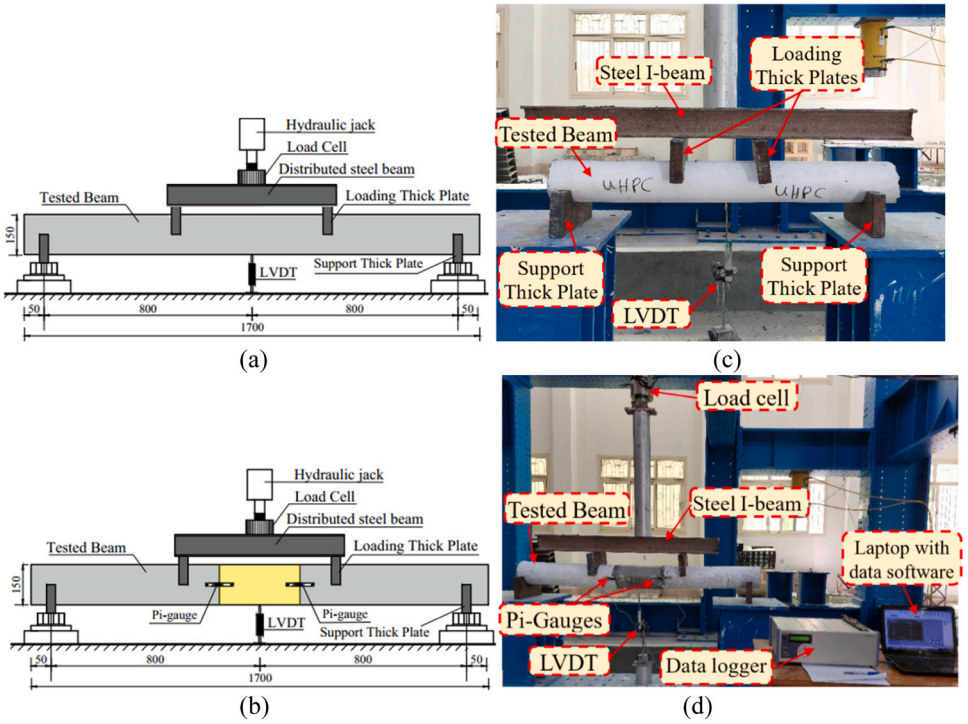

Fig. 5. Test set-up and details of the instrumentations: (a) schematic view of solid specimen, (b) image of the solid specimen during the test, (c) schematic view of precast specimen, and (d) image of the precast specimen during the test.

Table 3
Test results of the circular RC member with an intermediate connection.

Group	Specimen`s ID	Cracking Stage			Ultimate Stage			Elastic Stiffness Index (K)	K_B/K_0	Absorbed Energy (E)	Failure Mode
		P_{cr} (kN)	P_{crB}/P_{crB0}	Δ_{cr} (mm)	P_u (kN)	P_{uB}/P_{uB0}	Δ_{Pu} (mm)				
G1	C-NC	24.10	1.00	5.6	39.20	1.00	28.2	4.30	1.00	975.45	FC
	C-UHPC	30.05	1.25	5.8	51.51	1.31	33.2	5.18	1.20	1891.03	FC
	C-SHCC	32.60	1.35	6.0	57.8	1.47	30.15	5.43	1.26	1805.86	FC
G2	C-NC	24.10	1.00	5.6	39.20	1.00	28.2	4.30	1.00	975.45	FC
	U-0.027–15	22.31	0.93	5.7	32.05	0.82	21.9	3.91	0.91	614.97	F
	U-0.027–22.5	23.83	0.98	5.8	34.81	0.88	24.8	4.10	0.95	682.51	F
	U-0.027–30	28.52	1.17	6	36.22	0.92	26.0	4.75	1.10	944.04	DFS
G3	C-NC	24.10	1.00	5.6	39.20	1.00	28.2	4.30	1.00	975.45	FC
	U-0.031–15	25.42	1.05	5.82	35.15	0.89	24.5	4.36	1.01	749.92	DFS
	U-0.031–22.5	29.61	1.11	6.1	41.21	1.05	26.2	4.85	1.13	971.11	DFS
	U-0.031–30	32.94	1.14	6.12	43.27	1.10	27.0	5.38	1.25	1222.41	DFS
G4	C-NC	24.10	1.00	5.6	39.20	1.00	28.2	4.30	1.00	975.45	FC
	U-0.036–15	33.04	1.37	7.2	41.02	1.04	28.0	4.58	1.07	1084.05	F
	U-0.036–22.5	35.50	1.39	7.3	43.50	1.11	28.9	4.86	1.13	1259.81	F
	U-0.036–30	39.13	1.62	6.9	49.51	1.26	29.2	5.67	1.32	1478.59	F

Notes: P_{cr} = the cracking load; Δ_{cr} = deflection recorded at P_{cr}; P_U = the ultimate load; Δ_{Pu} = deflection recorded at P_U; K = elastic index; E = absorbed energy; F indicates the flexural failure mode; FC denotes the pure flexural failure; DFS = ductile flexural shear failure mode.

of flexural-shear cracks. The ultimate loads of U-0.031–15, U-0.031–22.5, and U-0.031–30 specimens were 35.15, 41.21, and 43.27 kN, respectively, as given in Table 3. All three specimens with intermediate connections had enhanced cracking loads. The ultimate load of the specimens with embedded lengths of 22.5*D* and 30*D* was higher than that of the C-NC by about 5% and 10%, respectively. It was discovered that the application of a 0.031 reinforcement ratio in UHPC connections with an embedded length of 150 mm changed the failure from flexural mode to flexural-shear mode as shown in Fig. 8.

Specimens U-0.036–15, U-0.036–22.5, and U-0.036–30 in the fourth group which was also parallel to the last two groups except it

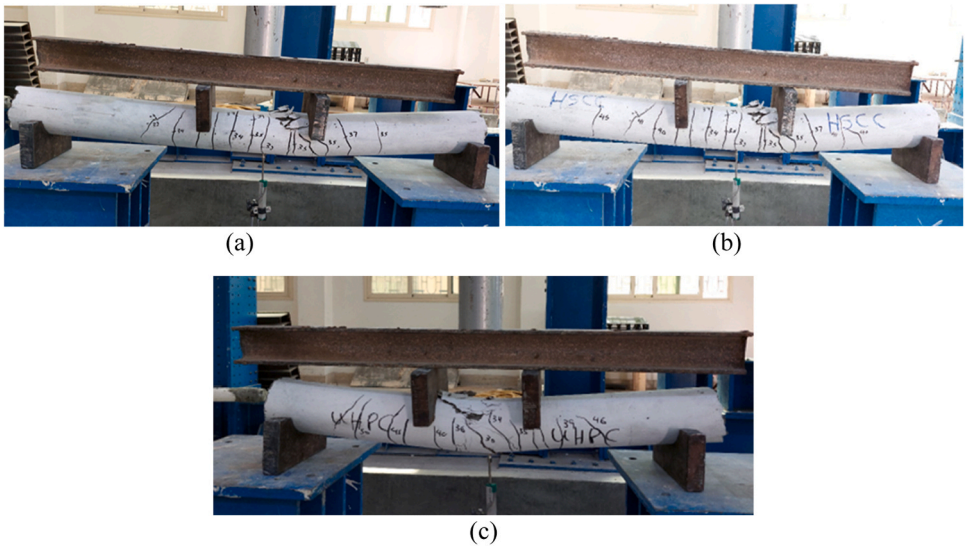

Fig. 6. Failure modes of specimens in Group G1: (a) C-NC, (b) C- SHCC, and (c) C-UHPC.

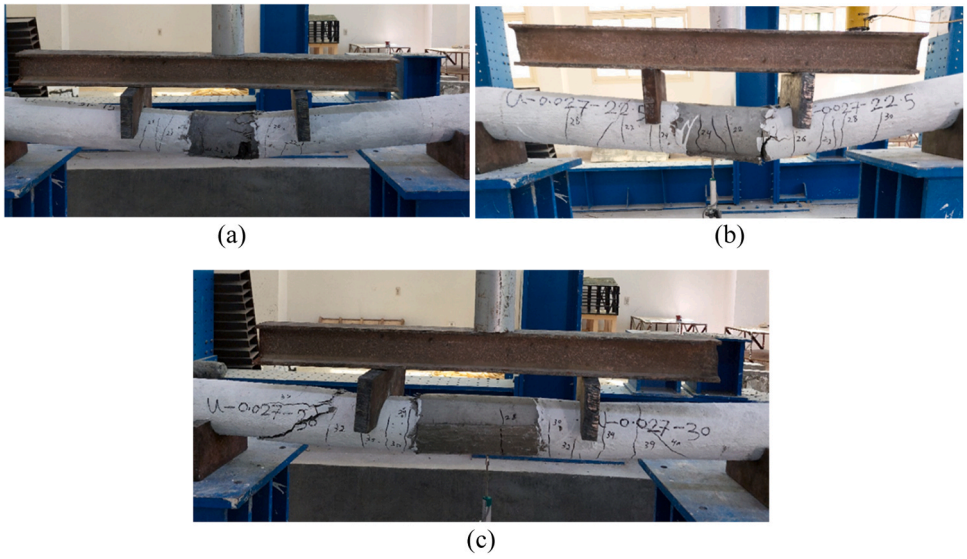

Fig. 7. Failure modes of specimens in Group G2: (a) U-0.027–15, (b) U-0.027–22.5, and (c) U-0.027–30.

had a reinforcement ratio of 0.036. The modes of failure in those specimens are shown in Fig. 9. The first flexural crack formed at the interface surface between the NC specimen panel and the UHPC side. The recorded cracking load was about 33.04, 35.5, and 39.13 kN for U-0.036–15, U-0.036–22.5, and U-0.036–30, respectively, which was higher than that of the control NC specimen by about 37%, 39% and 62%. A few flexural cracks developed from the lower tension side upward toward the upper side closing to the loading plates. The major flexural crack became wider as the load increased. As shown in Fig. 9, no significant flexural-shear cracks were formed in such types of specimens. Flexural failure mode associated with concrete crushing was observed in the vicinity of the compression zone between the connection and the NC panel. The load-carrying capacity was found to be enhanced by about 4–26% for this group, with respect to the tested parameters, compared to the control one as shown in Table 3.

3.2. Cracking and ultimate loads

The cracking and ultimate loads of all tested specimens are given in Table 3. The application of HPC such as SHCC or UHPC in the specimens in the first group increased the cracking loads by about 25% and 35%, respectively. The improvement was due to the addition of fibers which led to better tensile behavior of such concretes. The resistances of the specimens were improved by about 31% and 47% for C-SHCC and C-UHPC, respectively as shown in Fig. 10 (a).

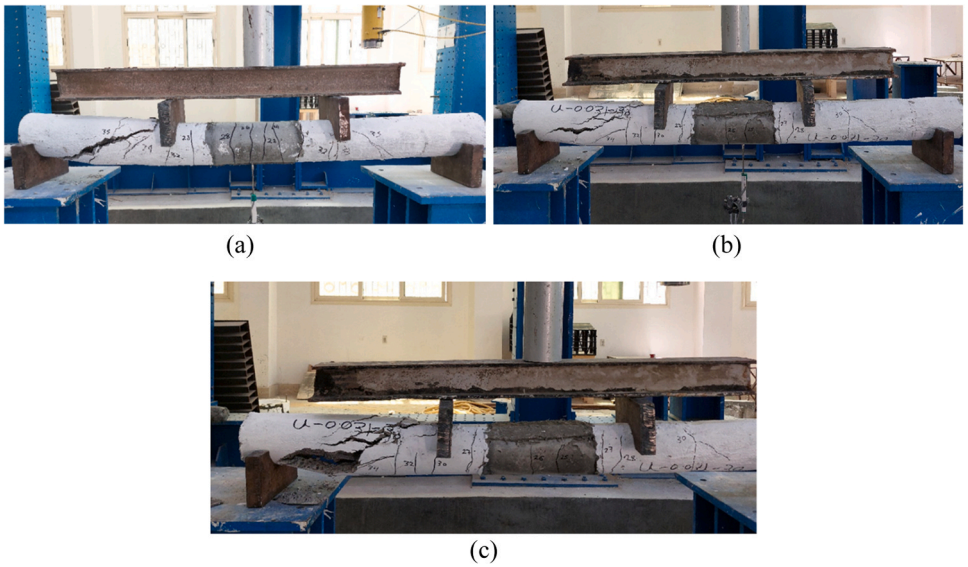

Fig. 8. Failure modes of specimens in Group G3: (a) U-0.031–15, (b) U-0.031–22.5, and (c) U-0.031–30.

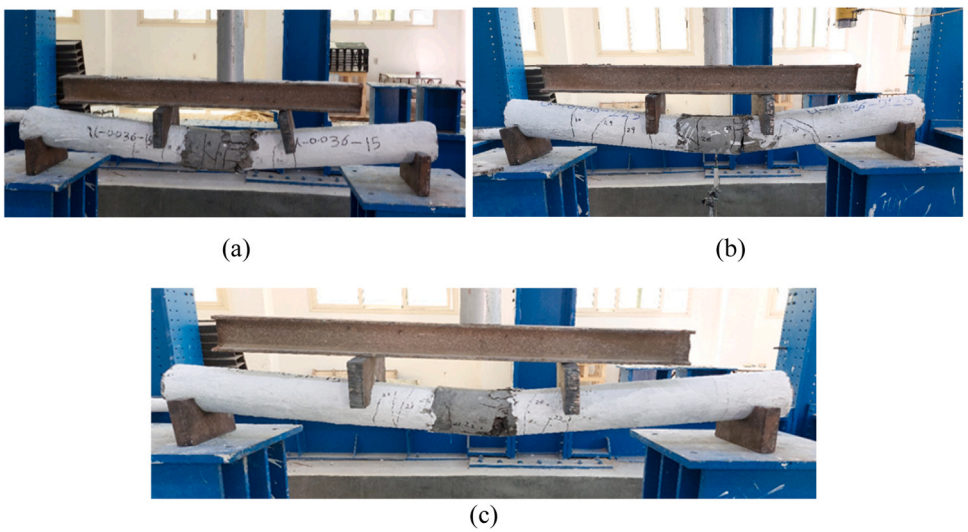

Fig. 9. Failure modes of specimens in Group G4: (a) U-0.036–15, (b) U-0.036–22.5, and (c) U-0.036–30.

The ultimate and cracking loads of the specimens in the second group did not increase compared with those of the control specimen without an intermediate connection. However, they were close to those of C-NC. It was observed that increasing both the lengths of the UHPC connection and reinforcement ratio improved the ultimate and cracking loads. The Group 3 showed the ratio of 0.031 had a higher cracking load than that of the control specimen. The enhancement was evaluated by about 5%, 11%, and 14% for when using embedded length of 15*D*, 22.5*D*, and 30*D* specimens, respectively, compared to the master specimen. The load-carrying capacity of the specimens U-0.031–22.5 and U-0.031–30 increased by about 5% and 10%, respectively as shown in Fig. 10 (a) and Table 3. However, the ultimate load of specimen U-0.031–15 was less than that of the control specimen.

For specimens in Group 3 with a 0.036 reinforcement ratio and embedded lengths of 15D, 22.5D, and 30D, the improvement in the cracking load over C-NC was estimated as 37%, 39% and 62%, respectively. The ultimate capacity of these specimens was enhanced by about 4%, 11%, and 26%, respectively, compared to the control NC specimen without an intermediate connection. The comparison given in Table 3 shows that the specimen with an intermediate connection and a reinforcement ratio of 0.036 possessed the highest bending strength.

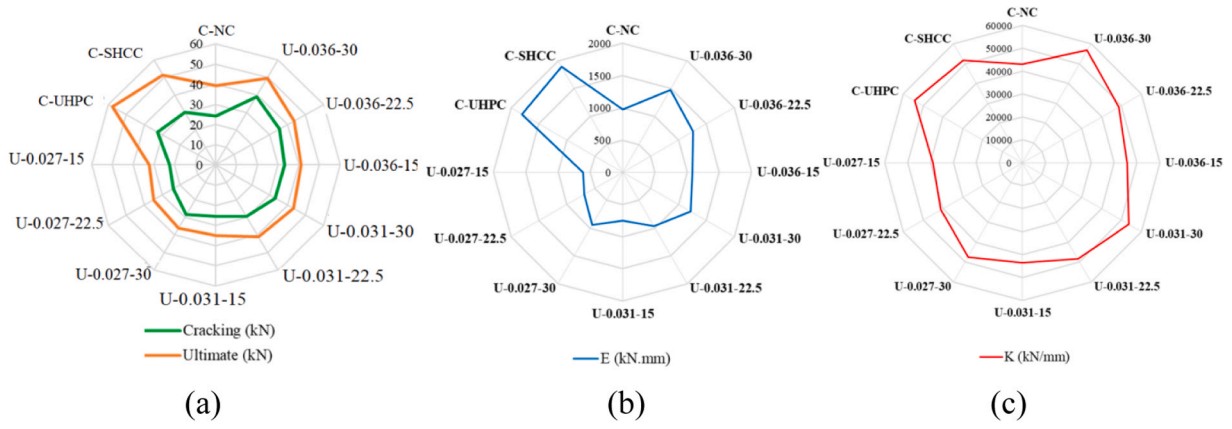

Fig. 10. Analysis of test results: (a) cracking and ultimate loads; (b) absorbed energy, and (c) Elastic index.

3.3. Absorbed energy

The absorbed energy (*E*) of the specimens has been calculated using the area under the experimental load-deflection curves. It was found that the new generation of HPCs resulted in a better improvement in the energy absorption capacity. Table 3 illustrates that the *E* values calculated for specimens made of UHPC and SHCC were 94% and 85% higher than that of the NC specimen (C-NC), respectively. Due to its higher strain hardening performance, the greater contribution to the absorbed energy is credited to the SHCC as shown in Fig. 10 (b).

The tested specimens in the second and third groups did not exhibit improvement in energy absorption compared to the control specimen. However, specimens with a 0.036 reinforcement ratio in the fourth group had enhanced energy absorption than the control one. Specimens with embedded lengths of 15D, 22.5D, and 30D had improved *E* value by about 11%, 29% and 52%, respectively, compared with the master NC specimen. Furthermore, it was found that the energy absorption capacity of the specimens increased as the embedded length increased. The increase in the embedded length provided additional stiffness to the intermediate connection, which improved the absorption capacity of the specimens. From the test results it is evident that to increase the absorption capacity of the beams with a shorter embedded length, higher reinforcement should be provided. However, for beams with a smaller reinforcement ratio, the embedded length should be increased to increase the absorption capacity of the beams.

3.4. Load deflection response and elastic index

Fig. 11 presents the diagrams of the load deflection for all tested specimens. The mid-span deflection values corresponding to the cracking and ultimate loads (Δ_{cr}) and (Δ_{Pu}) are provided in Table 3. The elastic stiffness indices (*K*) estimated from the load-displacement responses are also listed in Table 3.

For all tested specimens, the load-deflection relationship can be divided into three parts, such as linear, hardening, and softening behavior, as shown in Fig. 11. The first part corresponds to the uncracked stage starting from the zero loading up to the cracking load. In this context, all specimens behaved almost linearly. Then and with the first crack appearance, the elastic stiffness began to reduce. The second part corresponding to the cracked stage starts from the first cracking up to the maximum load with hardening behavior. The third part presents the softening behavior until the collapse as shown in Fig. 11.

As expected, due to the hardening performance of HPC, the load-deflection behavior of SHCC and UHPC specimens was enhanced compared to that made of NC as shown in Fig. 11 (a). The values of the elastic stiffness were enhanced by about 20% and 26% for specimens C-SHCC and C-UHPC, respectively compared to the NC specimens. Although C-SHCC had a lower ultimate capacity than the UHPC one, its ultimate deflection was larger than the UHPC one due to its strain-hardening characteristics as depicted in Fig. 11(a).

As shown in Fig. 11 (b), the load-deflection behavior of all specimens with intermediate connections was similar to that of the master NC specimen. Moreover, the application of a 0.027 reinforcement ratio could not sustain a higher load compared to solid NC one as tabulated in Table 3.

The use of reinforcing steel ratios of 0.031 and 0.036 in specimens in Groups G3 and G4 led to an increase in the load-carrying capacity and elastic index as depicted in Fig. 10 (b and c). A maximum increase in elastic stiffness was observed for the specimens with the largest embedded length. The elastic stiffness values were calculated as 5.38 and 5.67 for Group G3 and G4, respectively which are 25% and 32% higher than that of the control specimen. The specimens in these groups had a similar trend of variation in hardening or softening behavior with the master specimen; however, the deflections of specimens in Group G4 were larger.

4. Finite element modeling

The RC slender members made of NC and UHPC were modeled using a nonlinear three-dimensional FEMS software ABAQUS [25] to simulate their performance. The accuracy of the developed FEMs was verified by rivaling against the test obtains exploited in this research.

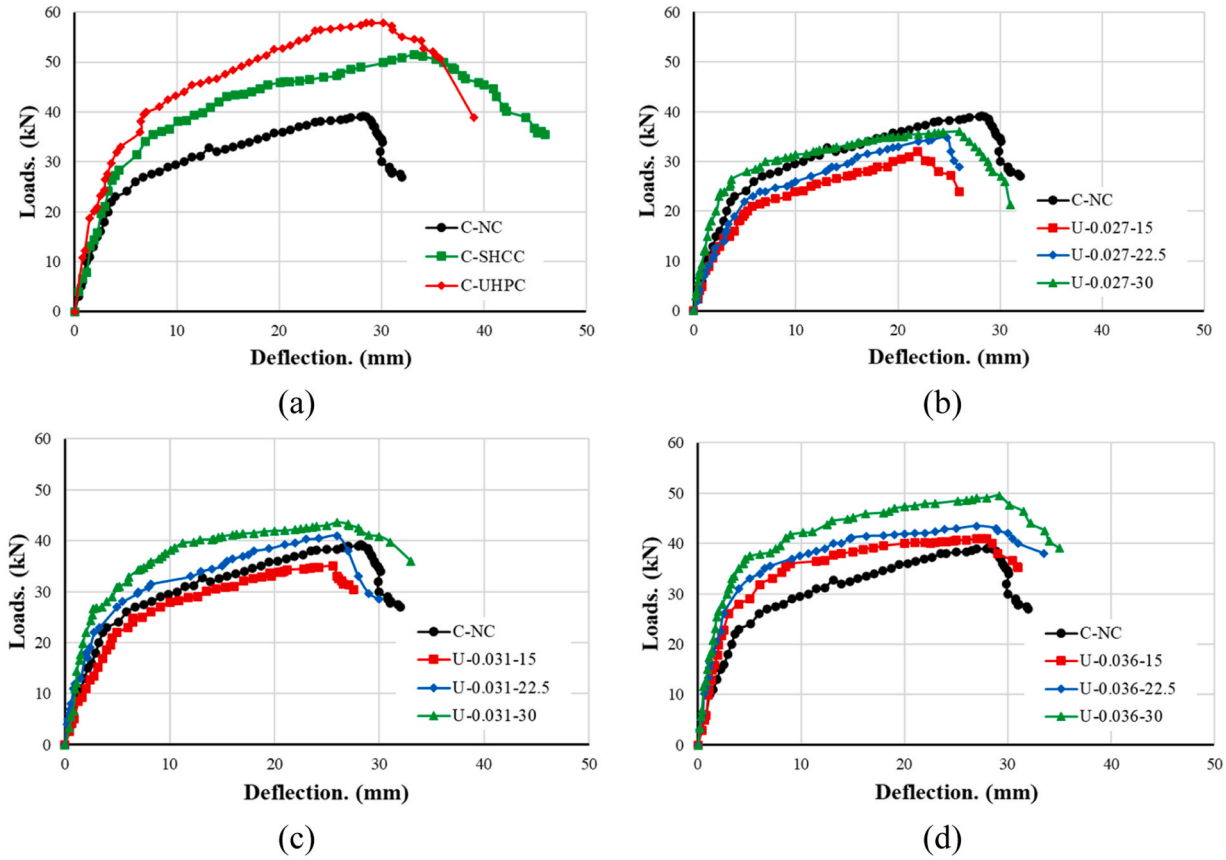

Fig. 11. Load-deflection relationships: (a) Group G1, (b) Group G2, (c) Group G3, and (d) Group G4.

4.1. Constitutive modeling of materials and sensitivity analysis

In the current study, the Concrete Damage Plasticity (CDP) model was adopted to represent the material behavior of concrete. The CDP model uses isotropic damage elasticity and tension plasticity and isotropic compression to model the nonlinear responses of concrete in tension and compression. It has been found that the CDP model generally predicts well the performance of RC specimens as reported by the authors [26,27]. The stress-strain relationships of NC and UHPC obtained from the test results were implemented in FE modeling, as shown in Fig. 2.

In order to save the computational cost, the actual experimentally measured stress-strain responses of steel elements were idealized as a piecewise linear curve as illustrated in Fig. 2(b). Both 8-mm and 10-mm diameter steel bars were used in this numerical modeling to simulate the ring steel stirrups and longitudinal reinforcement, respectively.

The stress-strain relationships of normal concrete and UHPC under compression were simulated using the models given by Carreira and Chu [28], and Chen and Graybeal [29], respectively. For concrete under tension, the idealized stress-strain curves obtained from the tests as shown in Fig. 2(e) were employed in the simulation. Sensitivity analyses were undertaken to select suitable factors such as the eccentricity (e), dilation angle (ψ), viscosity relaxation parameter (μ), the ratio of biaxial to uniaxial compressive stresses (f_{bo}/f_{co}), and ratio of the second stress invariant on the tensile to compressive meridian (K_c). For NC, the values of these parameters were taken as 0.1, 28°, 0, 1.16, 0.667, respectively, while these values were taken as 0.1, 36°, 0.000001, 1.16, 0.667 for UHPC and SHCC, respectively as recommended in previous studies [14,20,27].

4.2. Model set-up

Members from the first and fourth groups, except that with SHCC, were modeled using ABAQUS to validate the accuracy of the FEMs against the experimental results. As depicted in Fig. 12 (a), the eight-node element C3D8R was selected to model the concrete element. Four elastic zones were modeled to simulate both two loading zones and two supports as shown in Fig. 12 (a). To model the longitudinal rebars and transverse stirrups, two-node and linear truss element (T3D2) was utilized as depicted in Fig. 12 (b). An embedded element strategy with a perfect bond which is available in ABAQUS was utilized to model the contact between steel bars and concrete. The concrete component was treated as the host region while the steel bar was considered the embedded one. The C3D8R was used to model both the NC panel and UHPC intermediate connection as shown in Fig. 12 (c). The UHPC-NC Interfacial behavior was

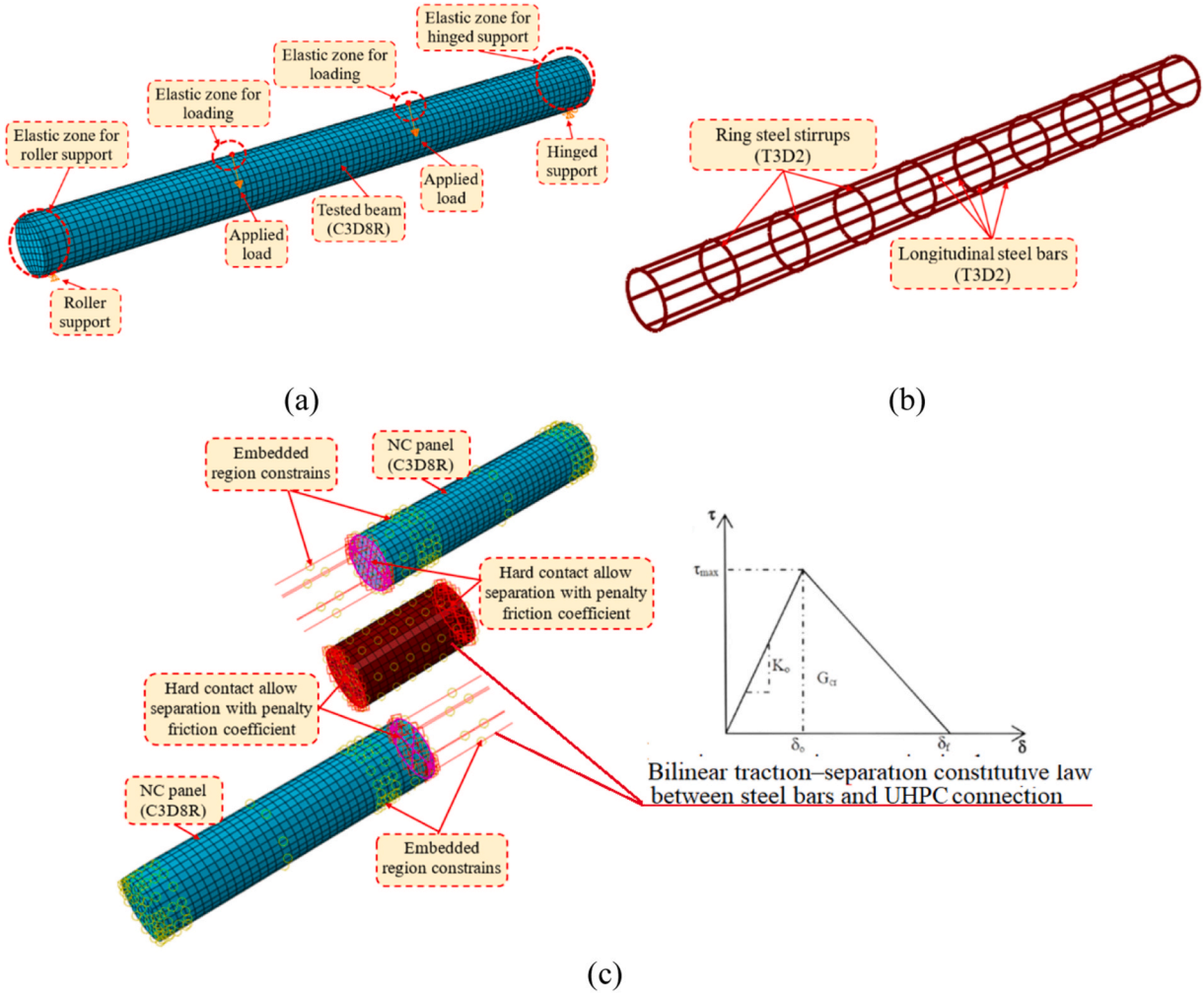

Fig. 12. Model set-up: (a) Types and boundary conditions for solid specimen, (b) Reinforcement details and element type, and (c) Types and interactions for the construction joint.

simulated using hard contact allowed separation with a penalty friction coefficient equaled to 0.6 [30]. The boundary condition of the members was modeled as simply supported as shown in Fig. 12 (a) and (c) in which the two-point loading system was applied to simulate the bending loads. Finally, the mesh size was taken as 25 mm which provided good results when compared with the experimental ones. The embedded steel-UHPC interaction has been realized with respect to Eligehausen [31]. This interaction was cohesive-damage as shown in Fig. 12. It is defined in terms of the effective and opening displacement (τ) and (δ), respectively. In Fig. 12, (K_0) is the associated stiffness, the local concrete bond resistance is τ_{max}, the ultimate opening displacement at failure is δ_f, beside the energy absorbed for first crack is (G_{cr}) which is equaled to the integration of the curve up to the peaked traction stage.

4.3. Numerical results and verifications

This section presents the numerical validation against experimental results in terms of the recorded results as summarized in Table 4, failure modes shown in Fig. 13, and load-deflection response depicted in Fig. 14. It is seen that the FEMs can accurately predict the experimentally observed failure patterns of the precast members under flexural load. The comparison of the load-deflection relationships predicted by the FEMs and experiment can be seen in Fig. 14. The agreement between the test and FEM predictions is good. As summarized in Table 4, the ultimate and cracking loads of the tested specimens are accurately captured by the FE model. The variance between experimental and numerical results is in an acceptable range. For Group 1, the average value of $P_{cr\ FE}/P_{cr\ EXP}$ ratios is 1.066 whereas the mean value of $P_{U\ FE}/P_{U\ EXP}$ is 1.043 with COV of 0.011. As shown in Table 4, for Group 4, the mean value of $P_{cr\ FE}/P_{cr\ EXP}$ ratios is 1.036 whereas the average value of $P_{U\ FE}/P_{U\ EXP}$ is 1.053.

Table 4
Comparison between numerical and experimental results.

Group	Specimen ID	P_{cr} (kN)			Δ_{cr} (mm)			P_u (kN)			Δ_{Pu} (mm)		
		EXP	FE	FE/ EXP	EXP	FE	FE/ EXP	EXP	FE	FE/ EXP	EXP	FE	FE/ EXP
G1	C-NC	24.1	26.3	1.09	5.6	5.4	0.96	39.2	42.5	1.08	28.2	27.5	0.97
	C-UHPC	32.6	33.8	1.03	6.0	5.8	0.96	57.8	58.9	1.01	30.1	29.8	0.99
	Avg			1.06			0.96			1.045			0.98
	SD			0.032			0.016			0.035			0.025
	COV			0.030			0.012			0.034			0.026
G2	U-0.027–15	22.31	23.21	1.04	5.7	5.61	0.98	32.05	33.17	1.03	21.9	20.85	0.95
	U-0.027–22.5	23.83	24.22	1.02	5.8	5.68	0.98	34.81	36.22	1.04	24.8	23.85	0.96
	U-0.027–30	28.52	29.56	1.04	6	5.82	0.97	36.22	37.05	1.02	26.0	25.41	0.98
	Avg			1.03			0.97			1.03			0.96
	SD			0.013			0.007			0.009			0.013
	COV			0.0064			0.0036			0.0045			0.0064
G3	U-0.031–15	25.42	26.22	1.03	5.82	5.68	0.98	35.15	36.74	1.05	24.5	23.85	0.97
	U-0.031–22.5	29.61	30.15	1.02	6.1	5.88	0.96	41.21	42.45	1.03	26.2	25.11	0.96
	U-0.031–30	32.94	34.01	1.03	6.12	5.98	0.98	43.27	45.22	1.05	27.0	26.30	0.97
	Avg			1.027			0.97			1.04			0.96
	SD			0.008			0.007			0.009			0.009
	COV			0.004			0.0036			0.0043			0.0044
G4	U-0.036–15	33.0	34.8	1.05	7.2	7.0	0.97	41.2	43.1	1.04	28.0	27.3	0.97
	U-0.036–22.5	35.5	37.0	1.04	7.3	7.1	0.97	43.5	46.3	1.06	28.9	27.8	0.96
	U-0.036–30	39.1	40.2	1.02	6.9	6.7	0.97	49.5	52.6	1.06	29.2	28.6	0.98
	Avg			1.036			0.972			1.053			0.97
	SD			0.015			0.001			0.012			0.010
	COV			0.015			0.001			0.011			0.010

EXP: Experimental; FE: Finite Element Model; Avg: Average; SD: Standard deviation; COV: Coefficient of variation.

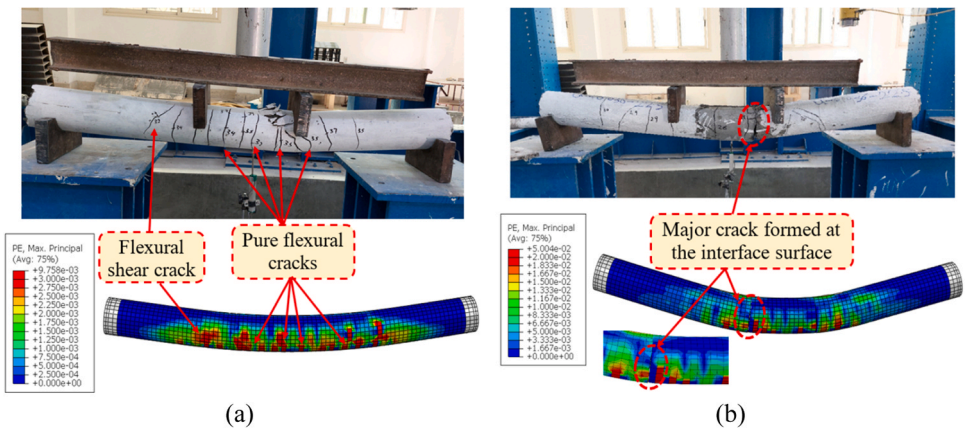

Fig. 13. Crack pattern for specimens: (a) C-NC and (b) U-0.036–22.5.

5. Conclusion

This paper has presented tests and finite element modeling of the flexural performance of RC specimens of circular cross-section with intermediate connections filled with HPC. The significance of the main parameters on the structural responses has been assessed, including the type of the filled concrete, the connection length, the reinforcement ratio, and the embedded length. Three-dimensional FEMs have been developed using ABAQUS to simulate the experimentally measured behavior of tested specimens. The following concluding remarks are provided:

1. The application of UHPC in circular RC members can significantly enhance flexural performance in both cracking and ultimate load stages. The load-carrying capacity of the specimens made of SHCC and UHPC was about 31% and 47%, respectively higher than that of the NC specimen.
2. Due to the strain-hardening characteristics, the higher contribution to the absorbed energy was credited to the C-UHPC and C-SHCC with 94% and 85% higher than C-NC, respectively.
3. The higher the reinforcement ratio and the longer the connection length, the higher the cracking load, ultimate load and the energy absorption capacity of the member.

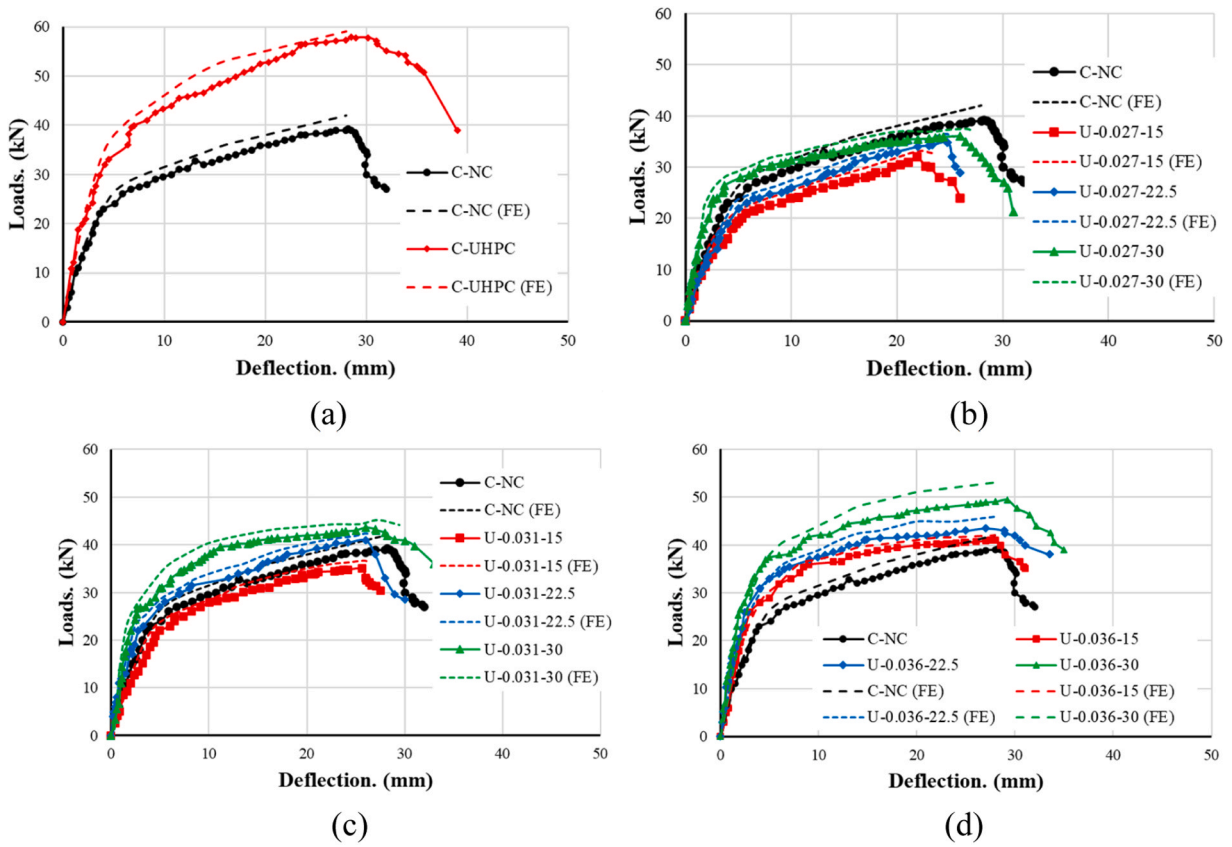

Fig. 14. Load-displacement responses obtained experimentally and numerically: (a) Group G1, (b) Group G2, (c) Group G3, and (d) Group G4.

4. Increasing the steel reinforcing ratio and the length of the UHPC connection remarkably improves the initial stiffness, cracking and ultimate loads, and the energy absorption capacity of circular RC specimens. The specimens with a 0.036 reinforcement ratio have the highest energy absorption capacity compared to specimens with other lower reinforcement ratios.
5. The tested specimens showed flexural failure mode during the test. However, using UHPC and SHCC improved the cracking behavior of the tested specimens. The increase in the first cracking load compared to the NC specimens was due to the higher tensile performance of UHPC.
6. The developed FEMs can accurately predict the experimentally measured performance of tested circular specimens.

Declaration of Competing Interest

The authors declare that they have no known competing financial interests or personal relationships that could have appeared to influence the work reported in this paper.

Data Availability

Data will be made available on request.

Acknowledgment

The help from technicians at Kafrelsheikh University is acknowledged. The authors acknowledge the first author for his self-funding contribution. In addition, the authors extend their appreciation to Researchers Supporting Project number (RSP2023R343), King Saud University, Riyadh, Saudi Arabia.

References

[1] C. Xu, D. Chen, S. Miramini, X. Liu, W. Xu, L. Zhang, Experimental fire performance assessment of a new type of prestressed composite circular precast concrete columns, Eng. Struct. 278 (2023), 115509.
[2] J. Zhou, M. Stümpel, C. Kang, S. Marx, Lap-spliced connections of steel and FRP bars in reinforced flexure concrete structures, Eng. Struct. 263 (2022), 114409.

[3] G. Gaurav, B. Singh, Experimental investigation for splice strength of deformed steel bars in normal-, medium-and high-strength recycled aggregate concrete, Constr. Build. Mater. 266 (2021), 121185.
[4] H. Dabiri, A. Kheyroddin, A. Faramarzi, Predicting tensile strength of spliced and non-spliced steel bars using machine learning-and regression-based methods, Constr. Build. Mater. 325 (2022), 126835.
[5] S. Ravasini, F. Vecchi, B. Belletti, A. Muttoni, Verification of deflections and cracking of RC flat slabs with numerical and analytical approaches, Eng. Struct. 284 (2023), 115926.
[6] X. Li, C. Lu, Y. Cui, L. Zhou, Study on the bond properties between steel bar and fiber reinforced concrete after high temperatures, Structures (2023) 889–902.
[7] M.T. Beni, M. Madhkhan, Experimental study on two innovative ductile moment-resisting precast concrete beam-column connections, Structures 39 (2022) 559–572.
[8] W. Xu, B. Ma, X. Duan, J. Li, Experimental investigation of seismic behavior of UHPC connection between precast columns and footings in bridges, Eng. Struct. 239 (2021), 112344.
[9] B. Graybeal, Ultra-high-performance concrete connections for precast concrete bridge decks, PCI J. 59 (4) (2014) 48–62.
[10] H.H. Hussein, S.M. Sargand, F.T. Al Rikabi, E.P. Steinberg, Experimental validation of optimized ultra-high-performance concrete shear key shape for precast pre-stressed adjacent box girder bridges, Constr. Build. Mater. 190 (2018) 178–190.
[11] Z. Fang, H. Fang, P. Li, H. Jiang, G. Chen, Interfacial shear and flexural performances of steel–precast UHPC composite beams: Full-depth slabs with studs vs. demountable slabs with bolts, Eng. Struct. 260 (2022), 114230.
[12] P. Ganesh, A.R. Murthy, Flexural fatigue strains of constituent materials in strengthened RC beams with UHPC strips, Int. J. Fatigue 167 (2023), 107351.
[13] M. Ahmed, Q.Q. Liang, A. Hamoda, Fiber element modeling of circular double-skin concrete-filled stainless-carbon steel tubular columns under axial load and bending, Adv. Struct. Eng. 25 (5) (2022) 1114–1135.
[14] A. Hamoda, F. Abdelazeem, M. Emara, Concentric compressive behavior of hybrid concrete–stainless steel double-skin tubular columns incorporating high performance concretes, Thin-Walled Struct. 159 (2021), 107297.
[15] H. Tan, Z. Hou, Y. Li, X. Xu, A flexural ductility model for UHPC beams reinforced with FRP bars, Structures 45 (2022) 773–786.
[16] H. Tian, Z. Zhou, B. Li, C. Jiang, Effect of strain gradient on the stress–strain relationship of FRP-confined ultra-high performance concrete, Compos. Struct. 304 (2023), 116371.
[17] H. Tian, Z. Zhou, Y. Wei, Y. Wang, Behavior of FRP-confined ultra-high performance concrete under eccentric compression, Compos. Struct. 256 (2021), 113040.
[18] H. Tian, Z. Zhou, Y. Wei, L. Zhang, Experimental and numerical investigation on the seismic performance of concrete-filled UHPC tubular columns, J. Build. Eng. 43 (2021), 103118.
[19] H. Tian, Z. Zhou, Y. Zhang, Y. Wei, Axial behavior of reinforced concrete column with ultra-high performance concrete stay-in-place formwork, Eng. Struct. 210 (2020), 110403.
[20] A. Hamoda, M. Emara, F. Abdelazeem, M. Ahmed, Experimental and numerical analysis of RC beams strengthened with ECC and stainless steel strips, Mag. Concr. Res. 75 (5) (2022) 251–270.
[21] A.E.-H. Khalil, E. Etman, A. Atta, M. Essam, Behavior of RC beams strengthened with strain hardening cementitious composites (SHCC) subjected to monotonic and repeated loads, Eng. Struct. 140 (2017) 151–163.
[22] M.I. Khan, S.U. Sial, G. Fares, M. ElGawady, S. Mourad, Y. Alharbi, Flexural performance of beams strengthened with a strain-hardening cementitious composite overlay, Case Stud. Constr. Mater. 17 (2022), e01645.
[23] A. Cabboi, O. Harrass, S.S. Gómez, M. Luković, Static and dynamic testing of delamination in hybrid SHCC/concrete beams, Compos. Struct. 281 (2022), 114961.
[24] A. Hassan, A.T. Baraghith, A.M. Atta, T.F. El-Shafiey, Retrofitting of shear-damaged RC T-beams using U-shaped SHCC jacket, Eng. Struct. 245 (2021), 112892.
[25] K. Hibbitt, I. Sorensen, ABAQUS Theory Manual, User Manual and Example Manual, Simuli,, Providence, RI, USA, 2000.
[26] A.A. Hamoda, B. Eltaly, M.S. Ghalla, Numerical investigation on reinforced concrete closed curved beams subjected to internal pressure strengthened with sustainable material, Erj. Eng. Res. J. (2023).
[27] G. Elsamak, M.I. Salama, A. Hamoda, Behavior of precast segmental beams made of high-strength concrete and ultra-high performance fiber concrete connected by shear keys technique, Arab. J. Sci. Eng. (2022) 1–17.
[28] D.J. Carreira, K.-H. Chu, Stress-strain relationship for plain concrete in compression, Acids Struct. J. 82 (6) (1985) 797–804.
[29] L. Chen, B.A. Graybeal, Modeling structural performance of second-generation ultrahigh-performance concrete pi-girders, J. Bridge Eng. 17 (4) (2012) 634–643.
[30] Z. Mahaini, F. Abed, Y. Alhoubi, Z. Elnassar, Experimental and numerical study of the flexural response of Ultra High Performance Concrete (UHPC) beams reinforced with GFRP, Compos. Struct. 315 (2023), 117017.
[31] R. Eligehausen, E.P. Popov, V.V. Bertero, Local Bond Stress-slip Relationships of Deformed Bars under Generalized Excitations, University of California, Berkeley, USA, 1982. UCB/EERC-83/23.